Supplementary Information

Behavior control of membrane-less protein liquid condensates with metal ion-induced phase separation

Kibeom Hong, Daesun Song, and Yongwon Jung*

Department of Chemistry, Korea Advanced Institute of Science and Technology, Daejeon 305-701, Korea. E-mail: ywjung@kaist.ac.kr

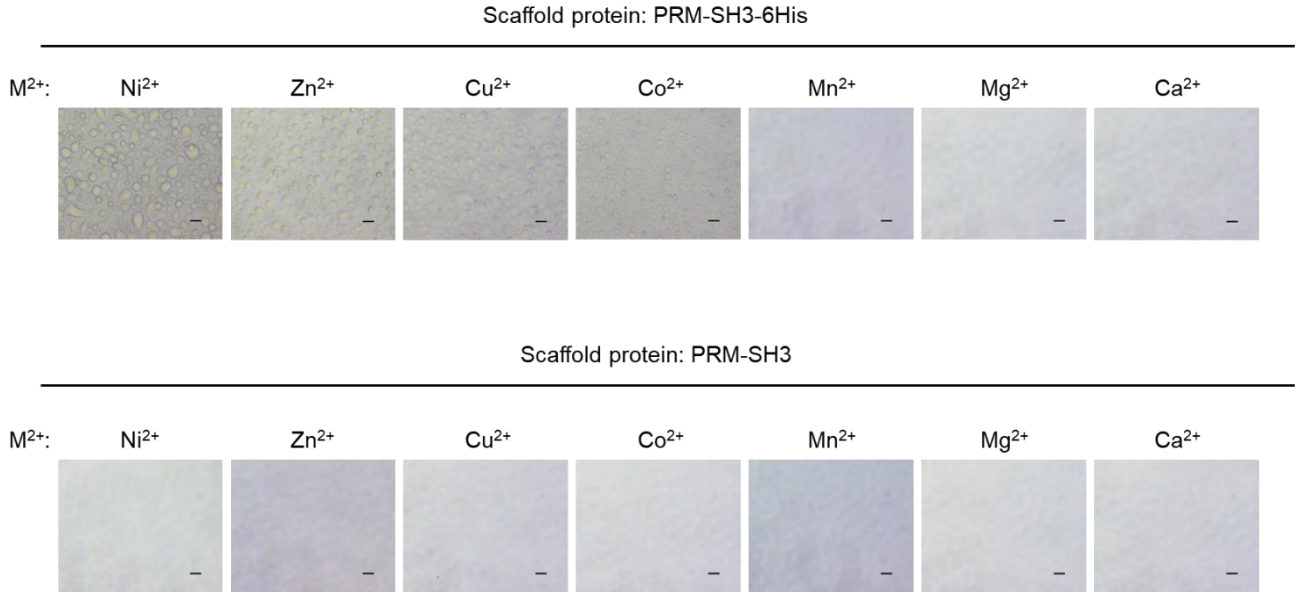

Supplementary Figure 1 Protein phase separation of PRM-SH3-6His (top) or PRM-SH3 without 6His (bottom) by various divalent metal ions. 100 μM protein and 100 μM metal ion were mixed, and optical images were obtained after 30 min upon divalent metal ion addition. Scale bars: 10 μm.

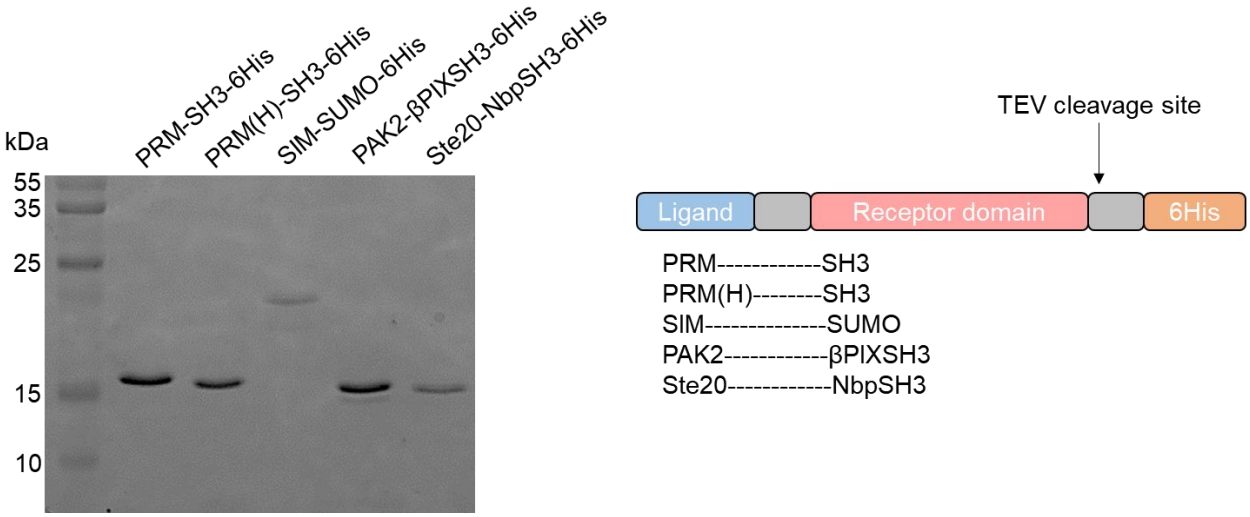

Supplementary Figure 2 Ligand-receptor-6His scaffold proteins. A SDS-PAGE image and schematic description of scaffold proteins are shown.

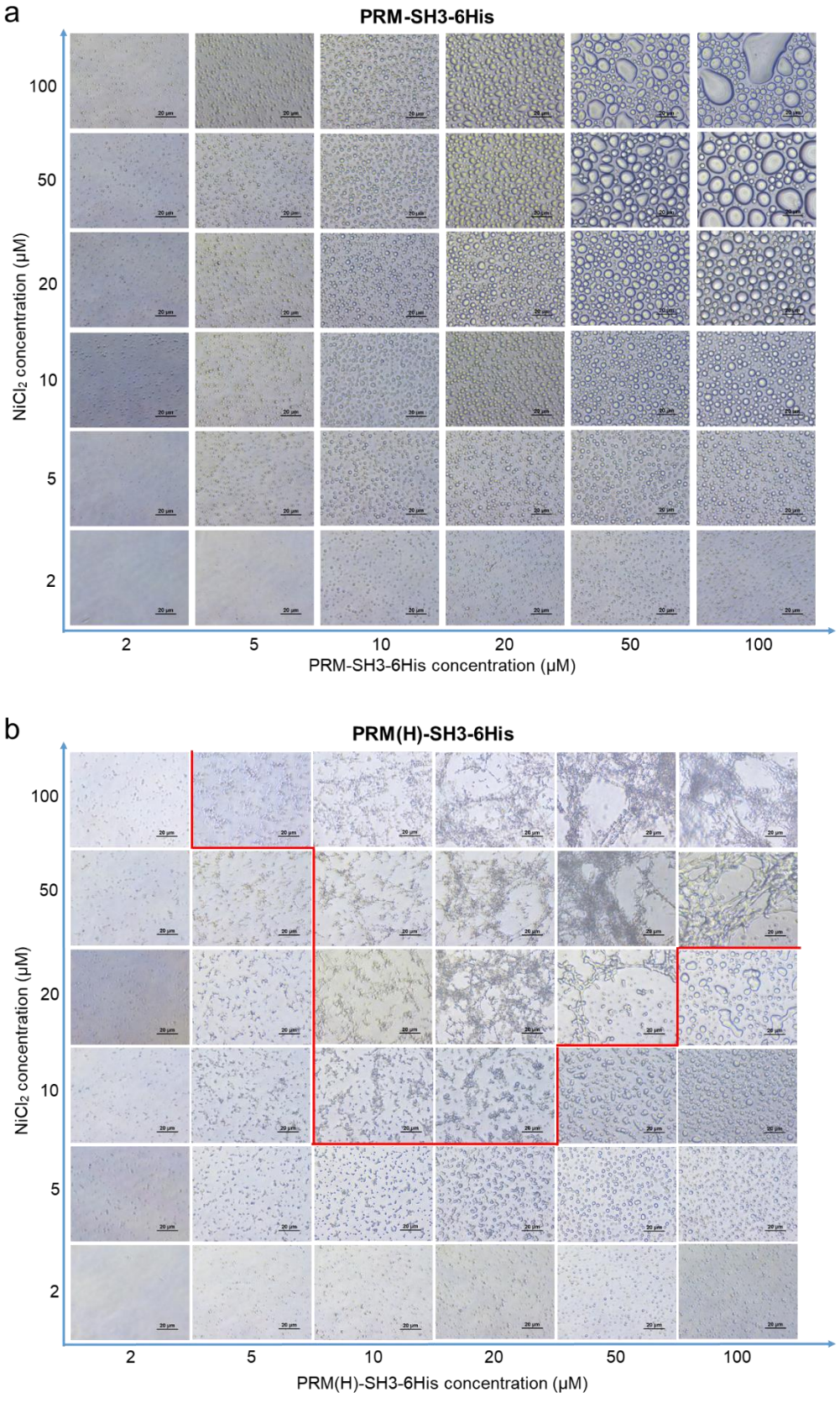

Supplementary Figure 3 Optical images of phase separation diagrams of five scaffold proteins. (continue)

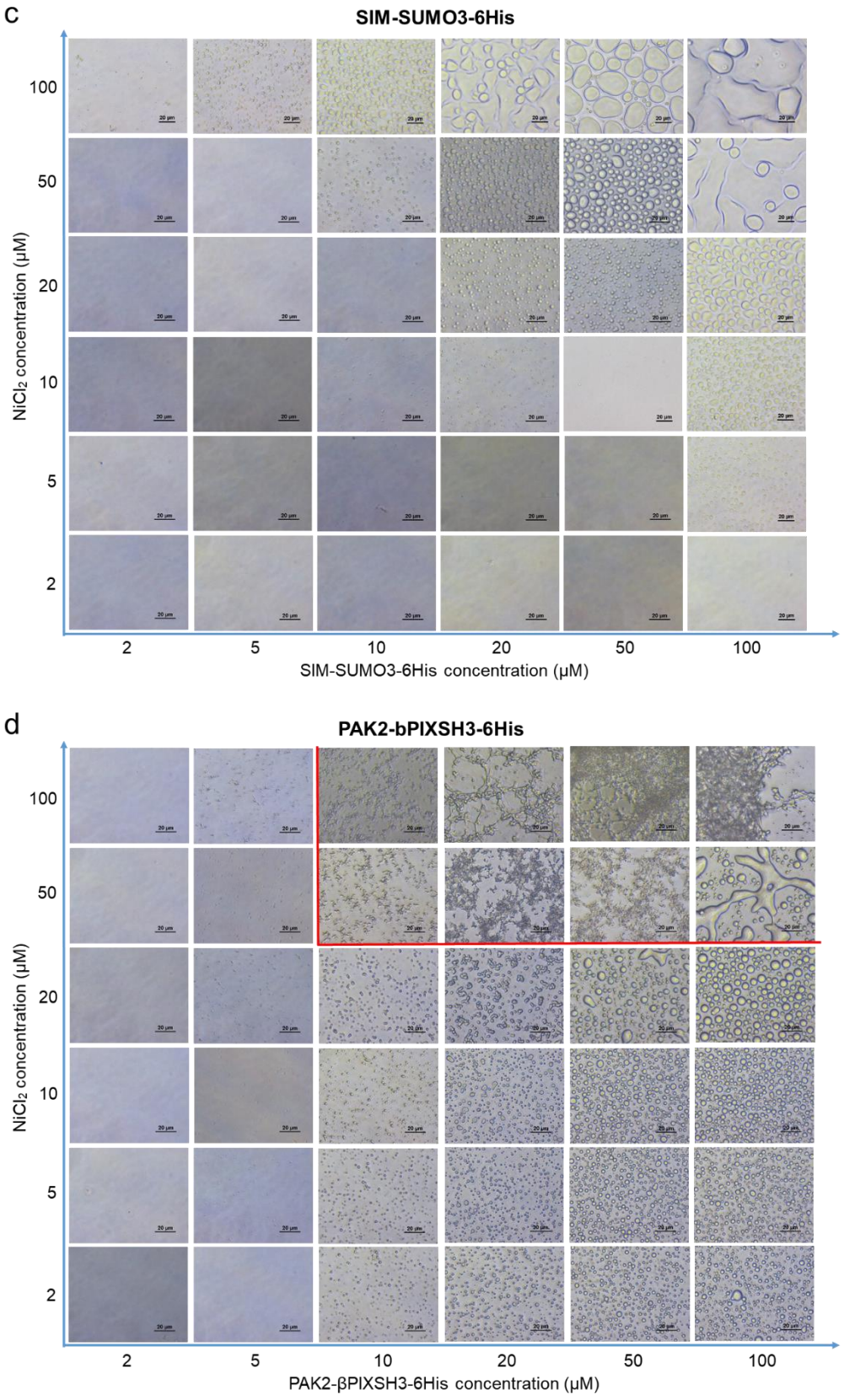

Supplementary Figure 3 Optical images of phase separation diagrams of five scaffold proteins. (continue)

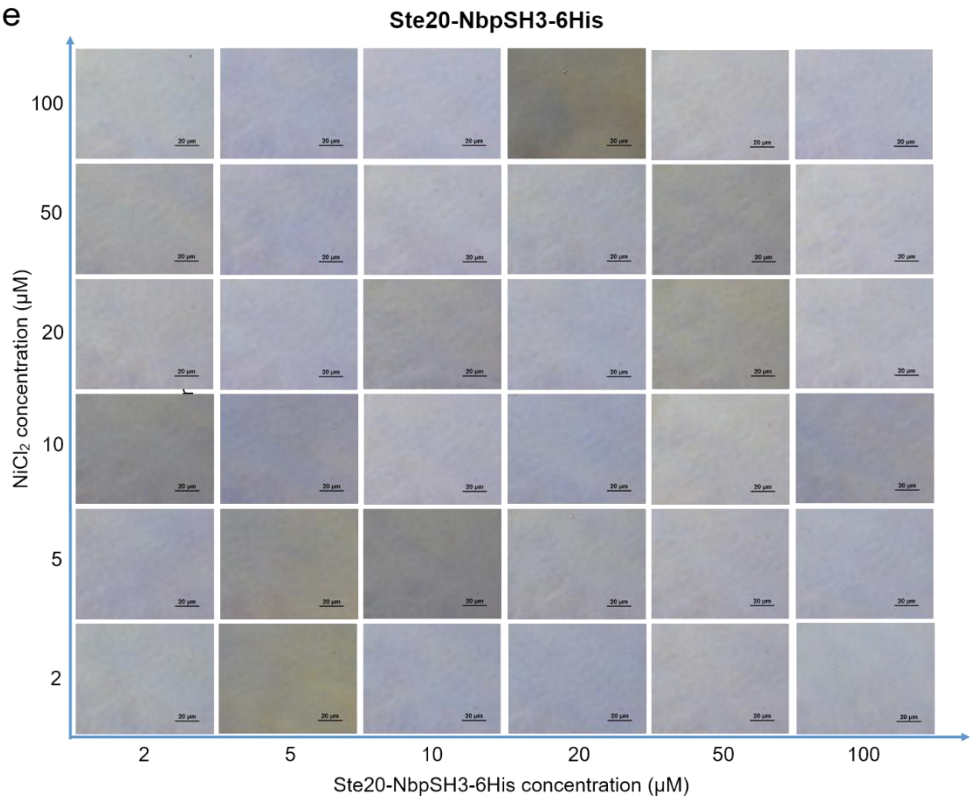

Supplementary Figure 3 Optical images of phase separation diagrams of five scaffold proteins. Droplets with gel-like structures are indicated with red lines. Phase diagram images of Fig. 1e. Scale bars: 10 μm. Images were taken after 24 h upon Ni^{2+} addition.

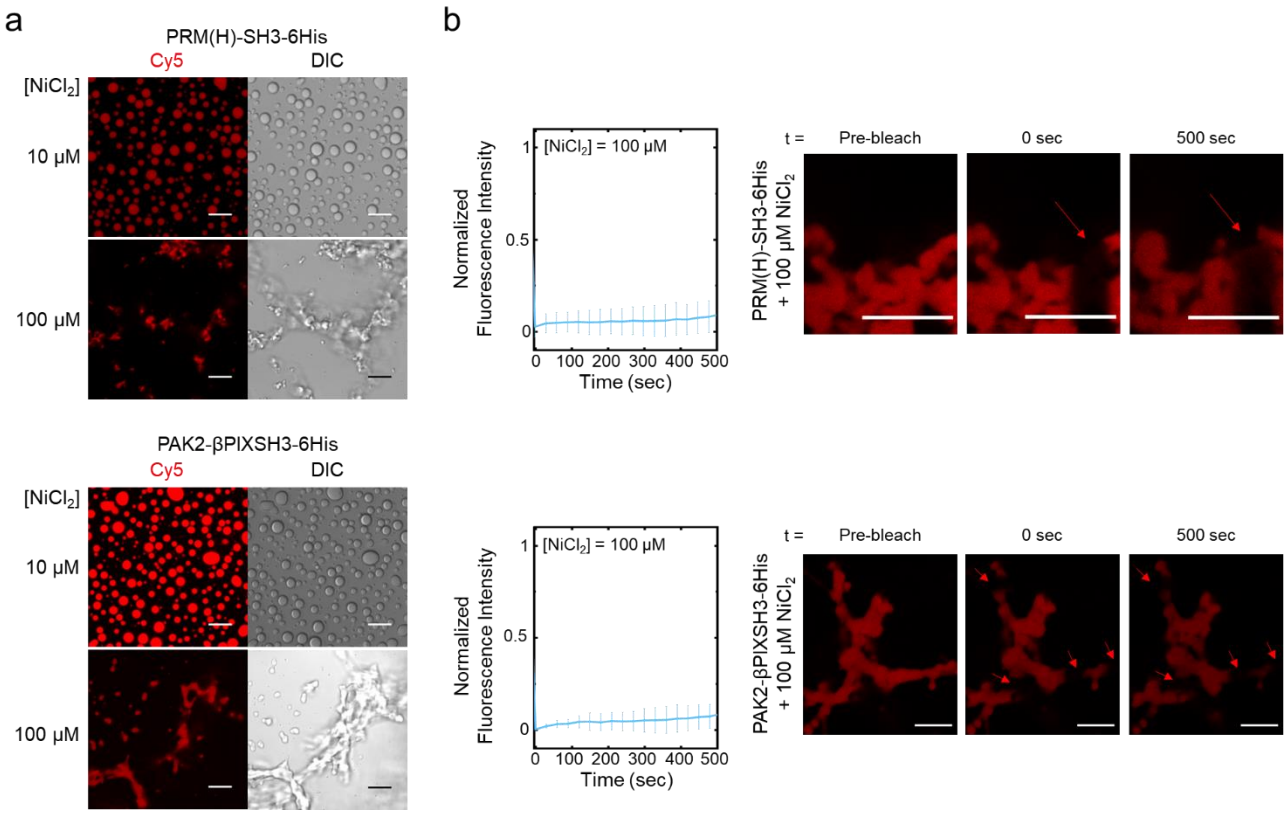

Supplementary Figure 4 Confocal and FRAP analyses of PRM(H)-SH3-6His (top) and PAK2-bPIXSH3-6His (bottom) protein condensates at $[Ni^{2+}]$ = 10 μM or 100 μM. (a) fluorescence and optical images of protein condensates. (b) FRAP recovery profiles and images of protein condensates at $[Ni^{2+}]$ = 100 μM. S.D. from triplicate experiments with at least 7 condensates. Scale bars: 10 μm. Condensates were analyzed after 12 h at 25 ºC upon Ni^{2+} addition.

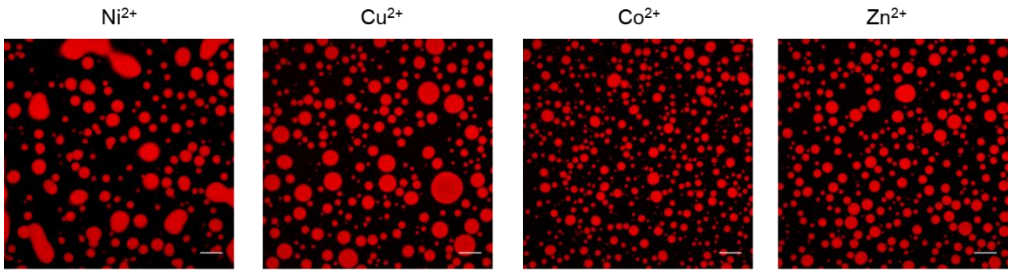

Metal ion	P.C.	S.D.
Ni^{2+}	29.6	3.33
Zn^{2+}	22.8	5.92
Co^{2+}	14.0	4.70
Cu^{2+}	13.2	5.26

Supplementary Figure 5 Fluorescence images of protein condensates containing Cy5-PRM-SH3-6His with four different metal ions. Scale bars: 10 μm. Partition coefficients (PCs) of the scaffold protein are indicated in the table below. S.D. from triplicate experiments with at least 302 condensates. Condensates were analyzed after 1 h at 25 ^{o}C upon Ni^{2+} addition.

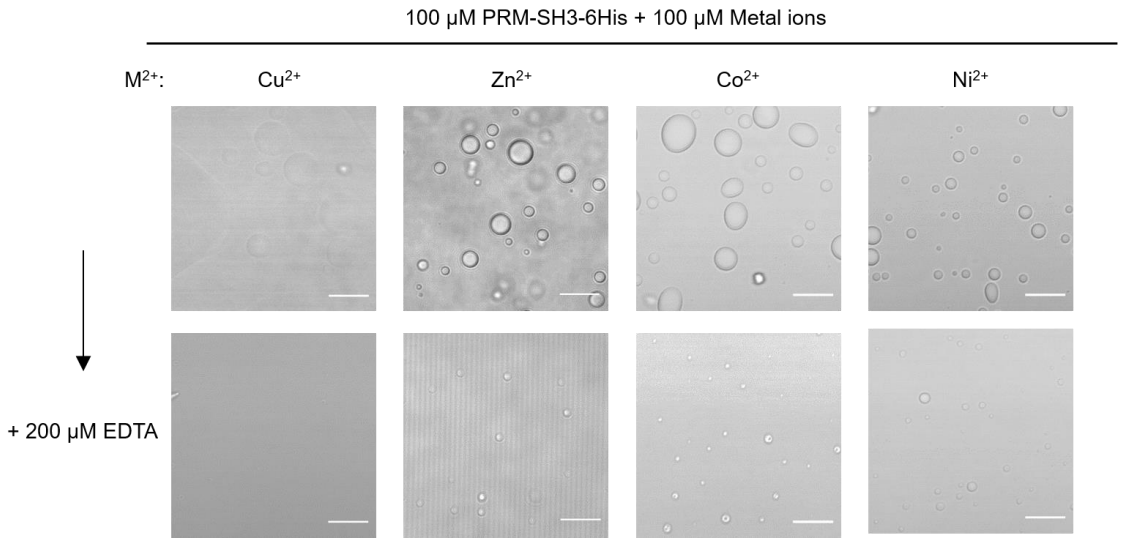

Supplementary Figure 6 EDTA-mediated dissolution of protein condensates formed with four different metal ions. Condensates were formed for 60 min (top images) and treated with EDTA for 5 min (bottom images). Scale bars: 10 μm.

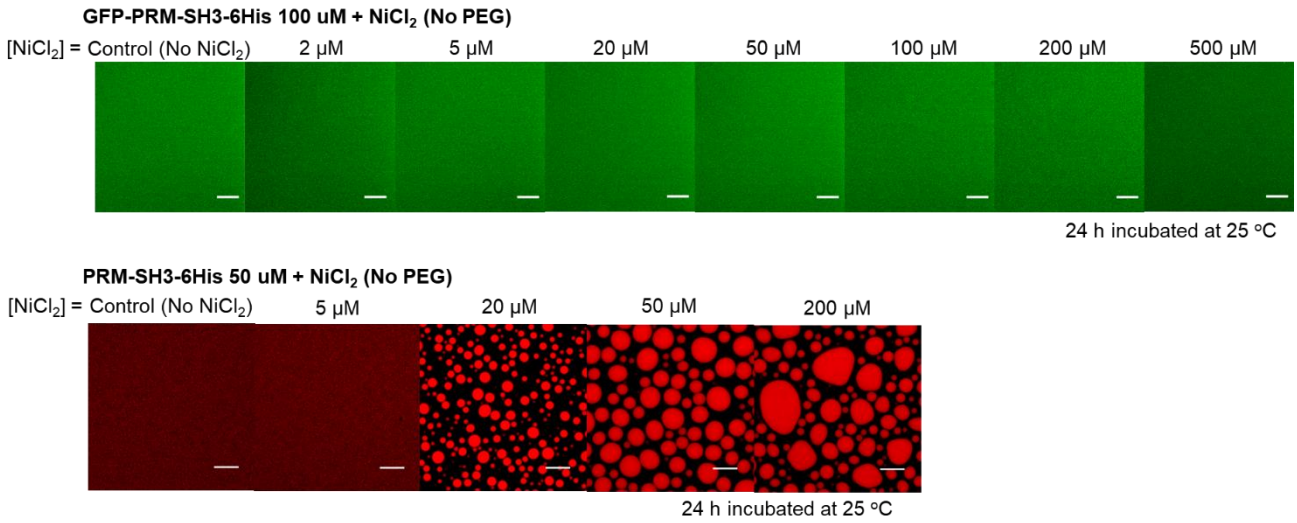

Supplementary Figure 7 Fluorescence confocal microscopy images of 100 µM GFP-PRM-SH3-6His (top) and 50 µM PRM-SH3-6His (bottom) with varying Ni^{2+} concentrations. Proteins and metal ions were mixed without PEG as conducted for DLS analyses. Scale bars: 10 µm

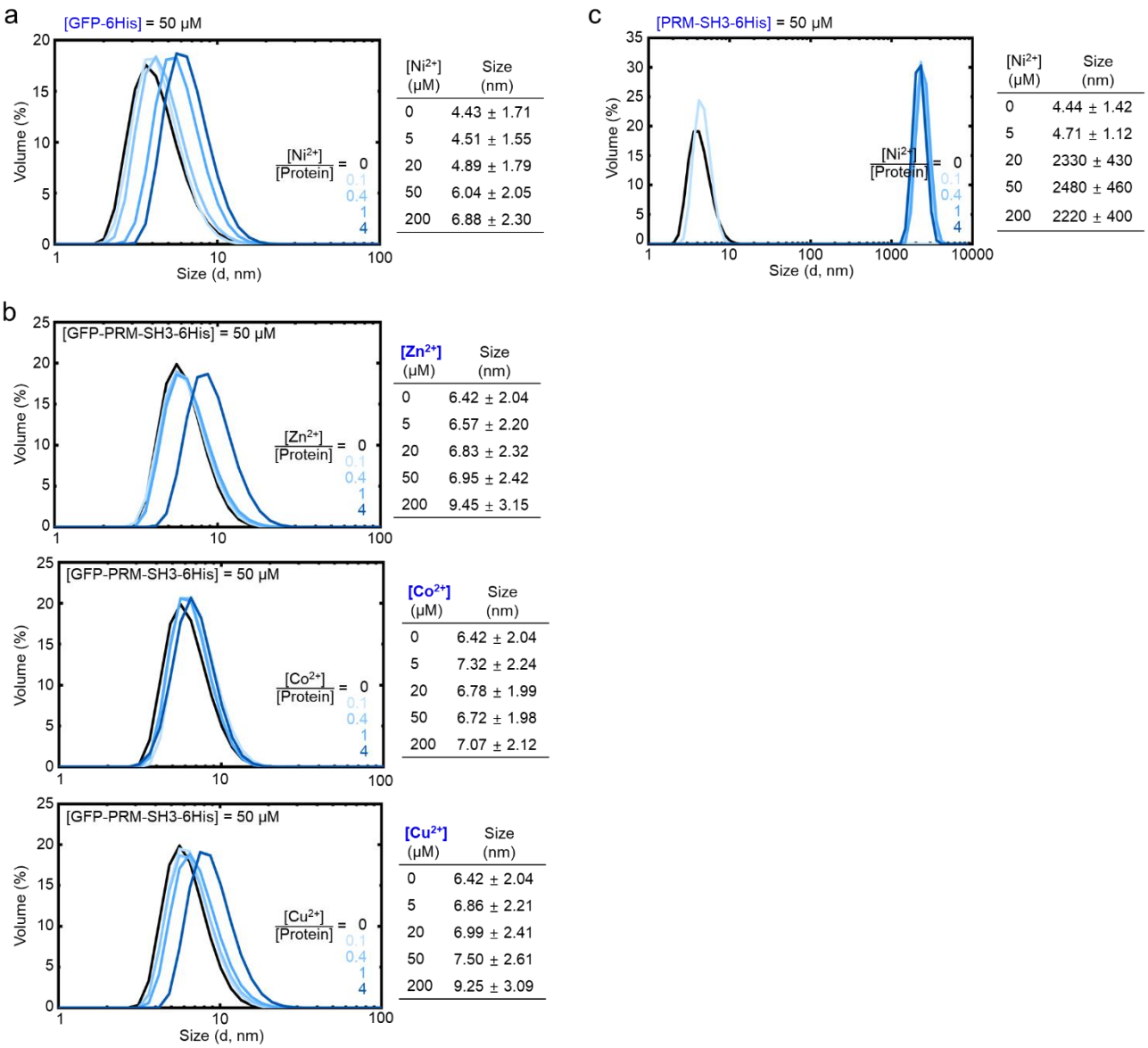

Supplementary Figure 8 DLS analysis of scaffold protein clustering by metal ions. (a) DLS size distribution profiles of GFP-6His with varying ratios of Ni^{2+}. Average sizes at different Ni^{2+} concentrations are indicated in the right table. (b) DLS size distribution profiles of GFP-PRM-SH3-6His with varying ratios of Zn^{2+}, Co^{2+}, and Cu^{2+}. (c) DLS size distribution profiles of PRM-SH3-6His with varying ratios of Ni^{2+}. S.D. n = 3.

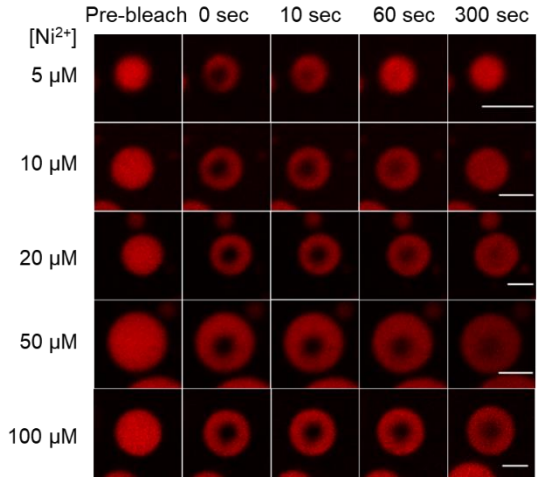

[Ni^{2+}] (µM)	Mobile Fraction (%)	S.D.	$t_{1/2}$ (sec)	S.D.
100	36.4	21.6	145	82.2
50	43.8	9.11	103	19.6
20	63.7	7.66	78.3	18.5
10	83.8	5.08	40.6	7.27
5	95.9	5.50	15.6	5.52

Protein = 100 µM
60 min incubation
Selected droplets 50 ~ 10 μm^2

Supplementary Figure 9 FRAP recovery images of 100 µM PRM-SH3-6His inside condensates with different Ni^{2+} concentrations (Fig. 2e). S.D. from triplicate experiments with at least 18 condensates. Scale bars: 10 µm. Condensates were analyzed after 1 h at 25 ºC upon Ni^{2+} addition.

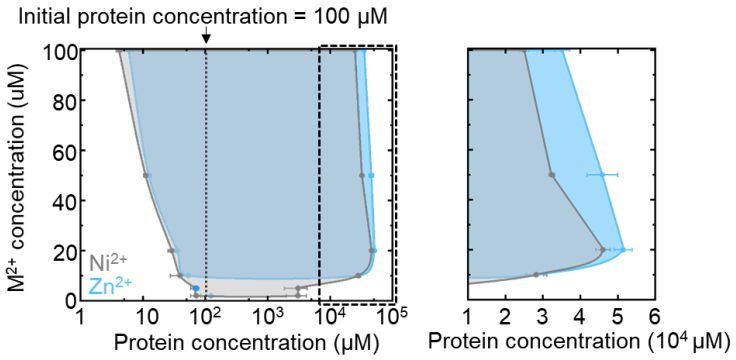

[M^{2+}] (μM)	Ni^{2+}		Zn^{2+}	
	[Dilute] (μM)	[Dense] (μM)	[Dilute] (μM)	[Dense] (μM)
2	71.5 ± 13.3	3060 ± 1080	-	-
5	68.1 ± 9.61	3070 ± 1230	-	-
10	39.3 ± 11.7	28200 ± 2820	53.6 ± 2.07	28000 ± 2160
20	28.9 ± 3.70	46000 ± 1910	35.3 ± 1.30	51400 ± 2360
50	11.0 ± 0.767	32300 ± 784	12.4 ± 1.24	45900 ± 4090
100	4.14 ± 0.417	25000 ± 1180	5.88 ± 0.86	35100 ± 2000

Supplementary Figure 10 The phase diagrams of PRM-SH3-6His with dense and dilute phase protein concentrations as a function of metal ion (M^{2+} = Ni^{2+} or Zn^{2+}) and PRM-SH3-6His concentrations. Left arms exhibit dilute phase concentrations and right arms for dense phase concentrations of the scaffold (PRM-SH3-6His) protein. The magnified version of the right arms (dash box in the left diagram) is drawn (right diagram). S.D. n = 3. The Ni^{2+} data are same as Fig. 2e, but included for better comparison with the Zn^{2+} data. Condensates were analyzed after 24 h at 25 ºC upon Ni^{2+} addition.

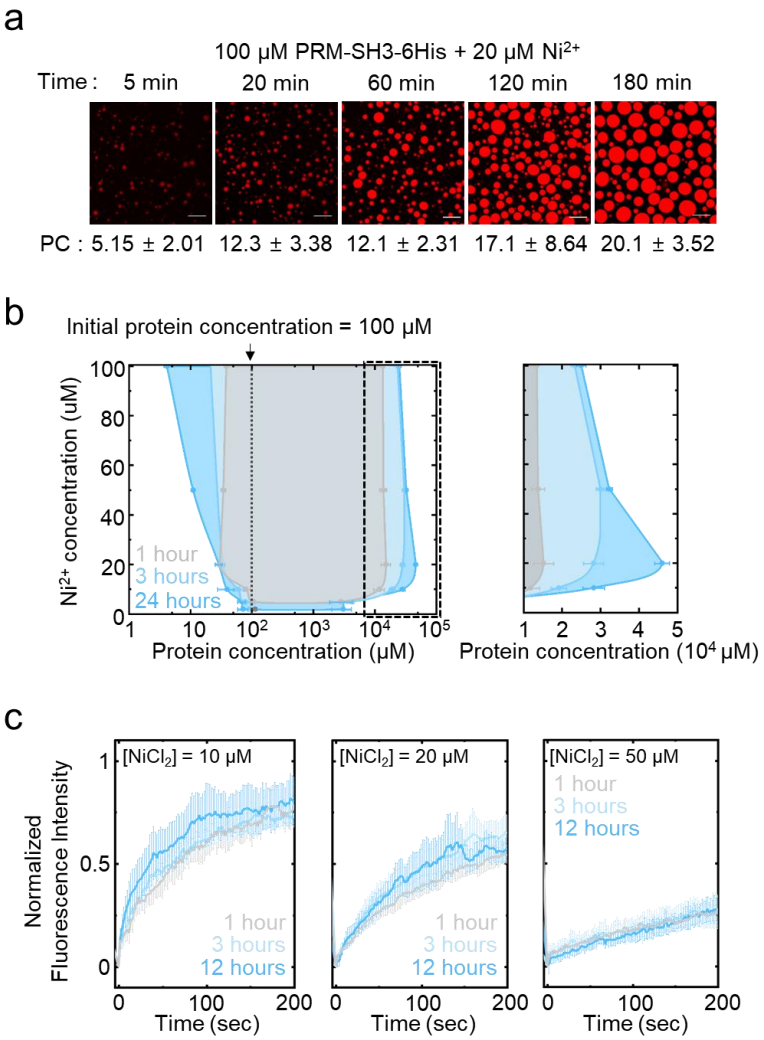

Supplementary Figure 11 Incubation time-dependent changes of protein condensate properties (a) Fluorescence images of PRM-SH3-6His condensates with varying incubation time. Scaffold PC values are indicated below. Scale bars: 10 μm. (b) The phase diagrams of PRM-SH3-6His with dense and dilute phase protein concentrations at incubation times 1 h, 3 h, and 24 h. The 24 h data are same as Fig. 2e, but included for better comparison with the 1 h and 3 h data. (c) FRAP recovery profiles of PRM-SH3-6His with different incubation time (1 h, 3 h, and 12 h) when [$NiCl_2$] = 10 μM (left), 20 μM (middle), and 50 μM (right). S.D. n = 3.

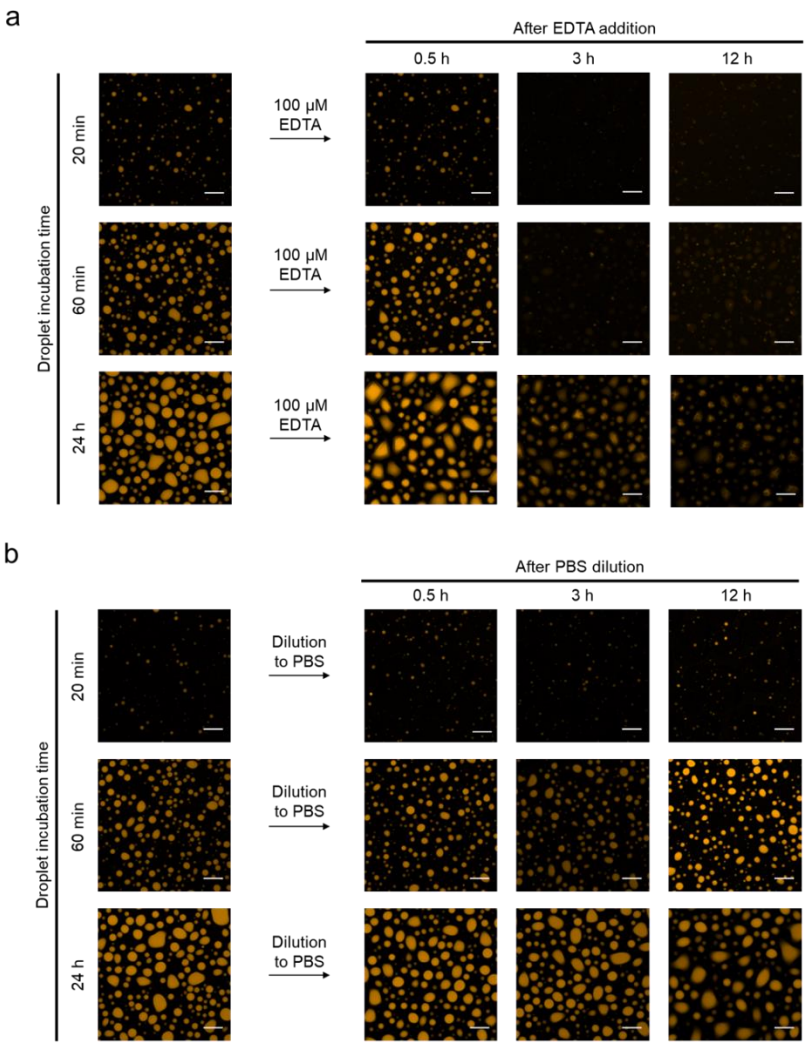

Supplementary Figure 12 Reversibility of protein condensates with different incubation time. (a) EDTA treatment to differently incubated Ni^{2+}-PRM-SH3-6His condensates. (b) PBS dilution of differently incubated Ni^{2+}-PRM-SH3-6His condensates. Scale bars: 10 μm.

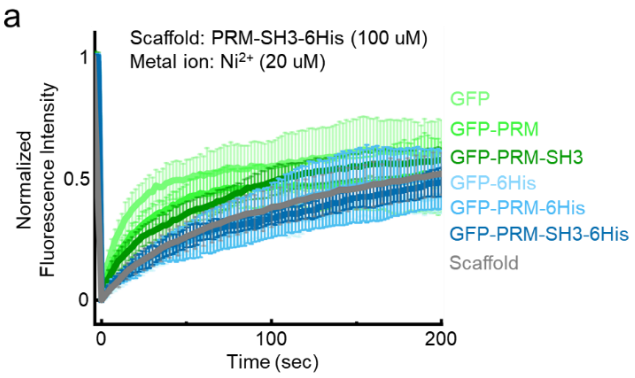

Client protein	Mobile Fraction (%)	S.D.	$t_{1/2}$ (sec)	S.D.
GFP	59.5	12.4	15	5.59
GFP-PRM	50.0	12.5	19	10.1
GFP-PRM-SH3	60.5	5.76	40.6	10.4
GFP-6His	47.9	9.05	58.6	10.8
GFP-PRM-6His	60.2	6.90	78.3	26.1
GFP-PRM-SH3-6His	54.1	4.29	64.2	8.54
Scaffold (PRM-SH3-6His)	63.7	7.66	78.3	18.5

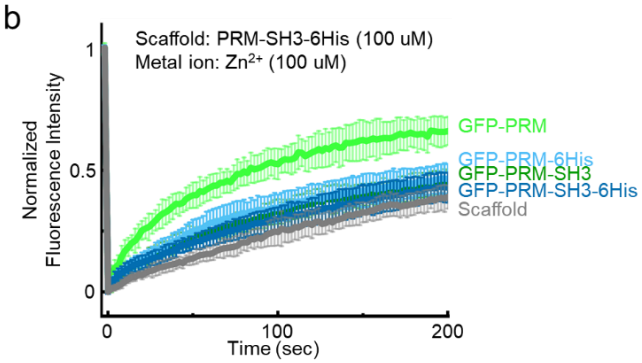

Client protein	Mobile Fraction (%)	S.D.	$t_{1/2}$ (sec)	S.D.
GFP-PRM	70.1	9.13	42.1	6.68
GFP-PRM-SH3	52.4	5.91	68.5	15.8
GFP-PRM-6His	53.0	5.75	63.6	10.4
GFP-PRM-SH3-6His	52.2	7.97	77.4	11.1
Scaffold (PRM-SH3-6His)	59.8	9.04	148	19.5

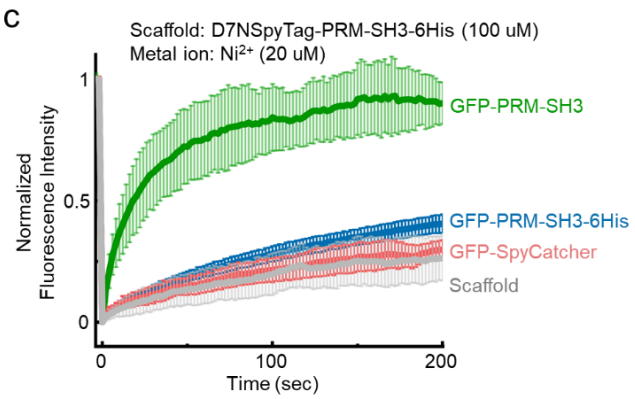

Client protein	Mobile Fraction (%)	S.D.	$t_{1/2}$ (sec)	S.D.
GFP-PRM-SH3	90.3	11.1	20.9	8.23
GFP-PRM-SH3-6His	47.1	4.13	73.1	9.46
GFP-SpyCatcher	35.0	4.74	75.2	34.9
Scaffold (D7NSpyTag-PRM-SH3-6His)	34.2	14.5	80.0	39.8

Supplementary Figure 13 Diffusivities of GFP-fused client protein variants inside condensates. (a) FRAP recovery profiles of GFP-fused clients inside PRM-SH3-6His condensates with Ni^{2+}. (b) FRAP recovery profiles of GFP-fused clients inside PRM-SH3-6His condensates with Zn^{2+}. (c) FRAP recovery profiles of GFP-fused clients inside D7NSpyTag-PRM-SH3-6His condensates with Ni^{2+}. S.D. from triplicate experiments with 12~31 condensates. Condensates were analyzed after 1 h at 25 ºC upon Ni^{2+} addition.

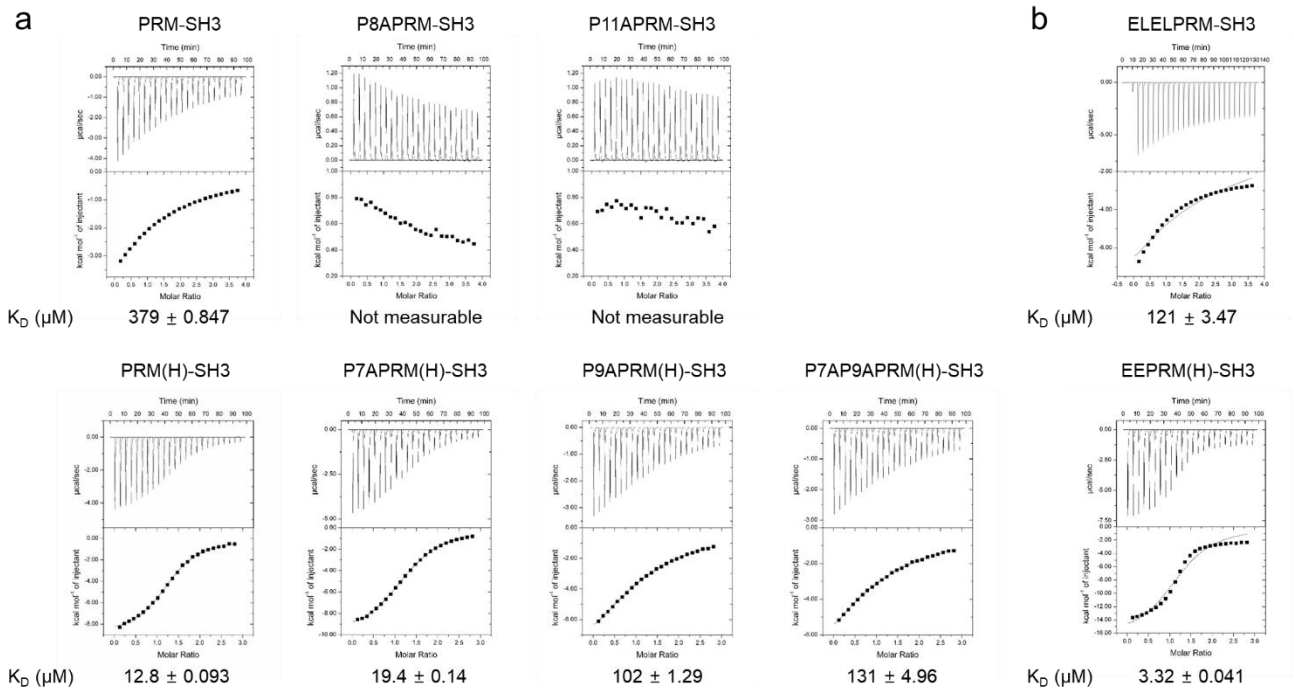

Ligand	[Syringe] (μM)	[Cell] (μM)	K_d (μM)	Affinity fold Increase
PRM	3500	175	379 ± 0.847	1
P8A	4000	200	N.A.	-
P11A	4000	200	N.A.	-
ELELPRM	3000	150	121 ± 3.47	3.13
PRM(H)	1500	100	12.8 ± 0.093	29.6
P7APRM(H)	1500	100	19.4 ± 0.14	19.5
P9APRM(H)	1500	100	102 ± 1.29	3.70
2APRM(H)	1500	100	131 ± 4.96	2.89
EEPRM(H)	1500	100	3.32 ± 0.041	114

Supplementary Figure 14 ITC thermograms of various (a) PRM variants and (b) PRM(H) variants (syringe) addition to the SH3 domain (cell). PRM and PRM(H) variant peptides were chemically synthesized, while SH3 was recombinantly produced in *E. coli*. P8APRM/SH3 and P11APRM/SH3 thermograms were not suitable to fit for K_D calculation due to their low binding affinities. Titration concentrations and relative binding affinities compared to the PRM/SH3 interaction are given in the below table.

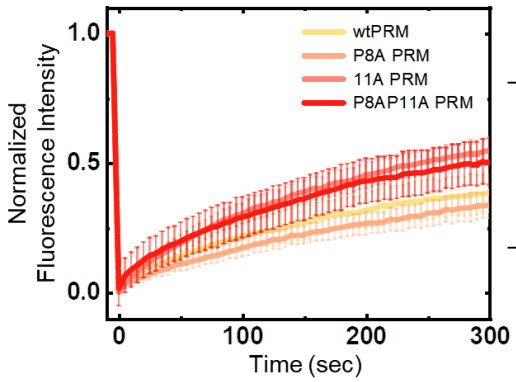

Protein	Mobile Fraction (%)	S.D.	$t_{1/2}$ (sec)	S.D.
PRM-SH3-6His	43.8	9.11	103	19.6
P8APRM-SH3-6His	48.4	8.68	169	43.0
P11APRM-SH3-6His	65.9	4.22	117	22.3
P8AP11APRM-SH3-6His	60.2	6.67	115	22.5

Protein = 100 μM
$NiCl_2$ = 50 μM
60 min incubation

Supplementary Figure 15 FRAP recovery profiles of Pro-to-Ala mutated PRM-SH3-6His scaffold proteins inside condensates. S.D. from triplicate experiments with at least 17 condensates. Condensates were analyzed after 1 h at 25 ºC upon Ni^{2+} addition.

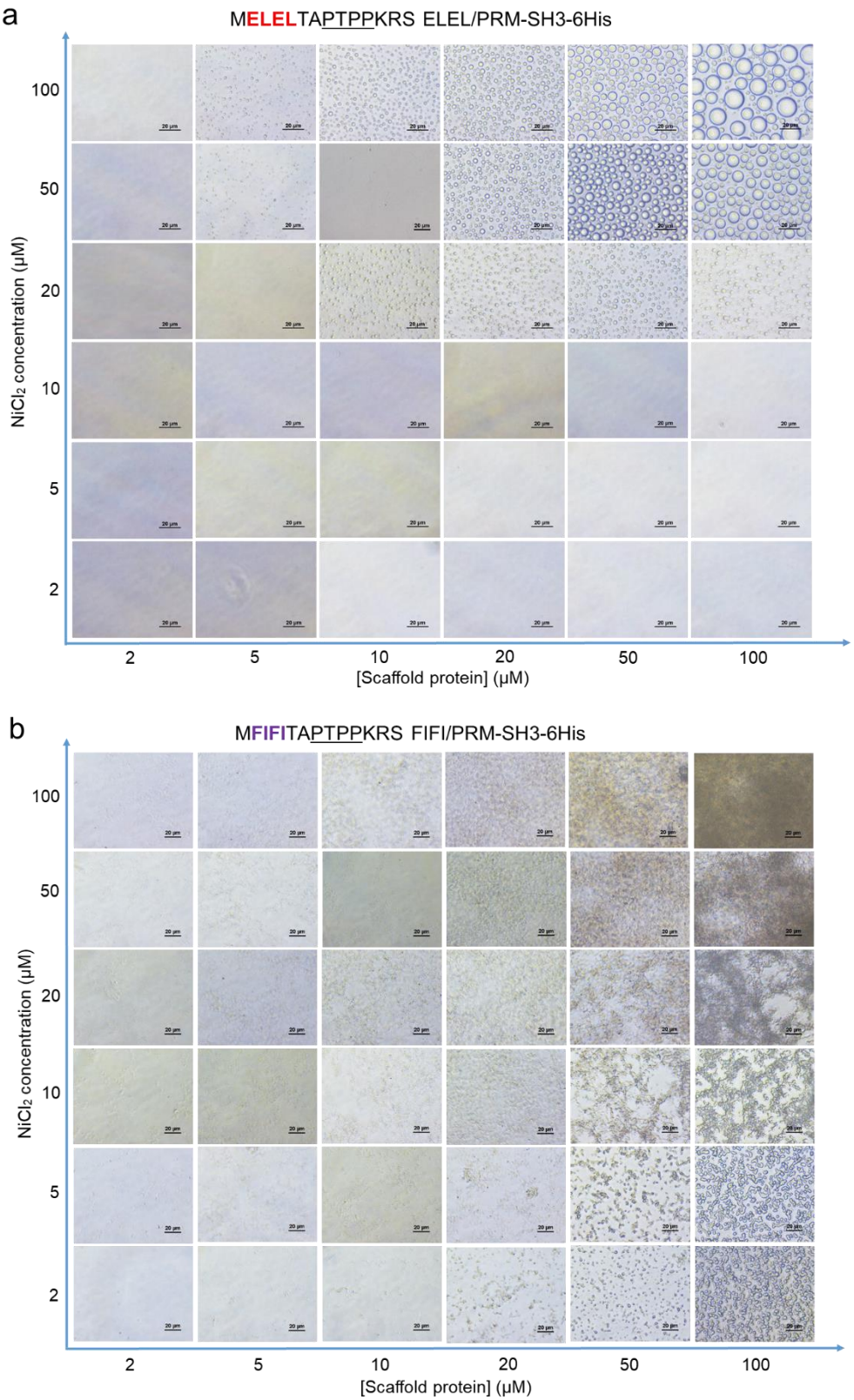

Supplementary Figure 16 Optical images of phase separation diagrams of ligand mutated scaffold proteins. (continue)

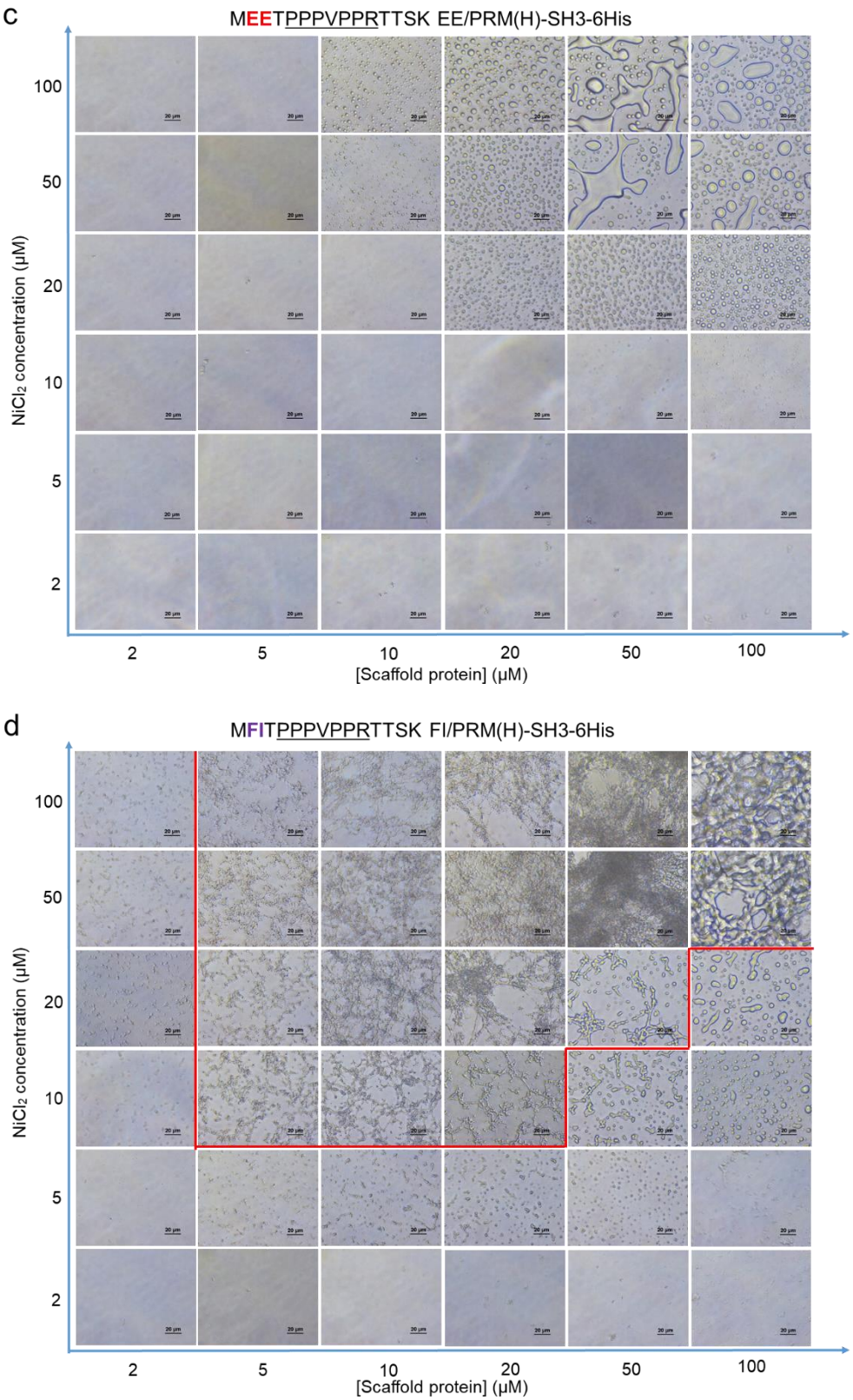

Supplementary Figure 16 Optical images of phase separation diagrams of ligand mutated scaffold proteins. (continue)

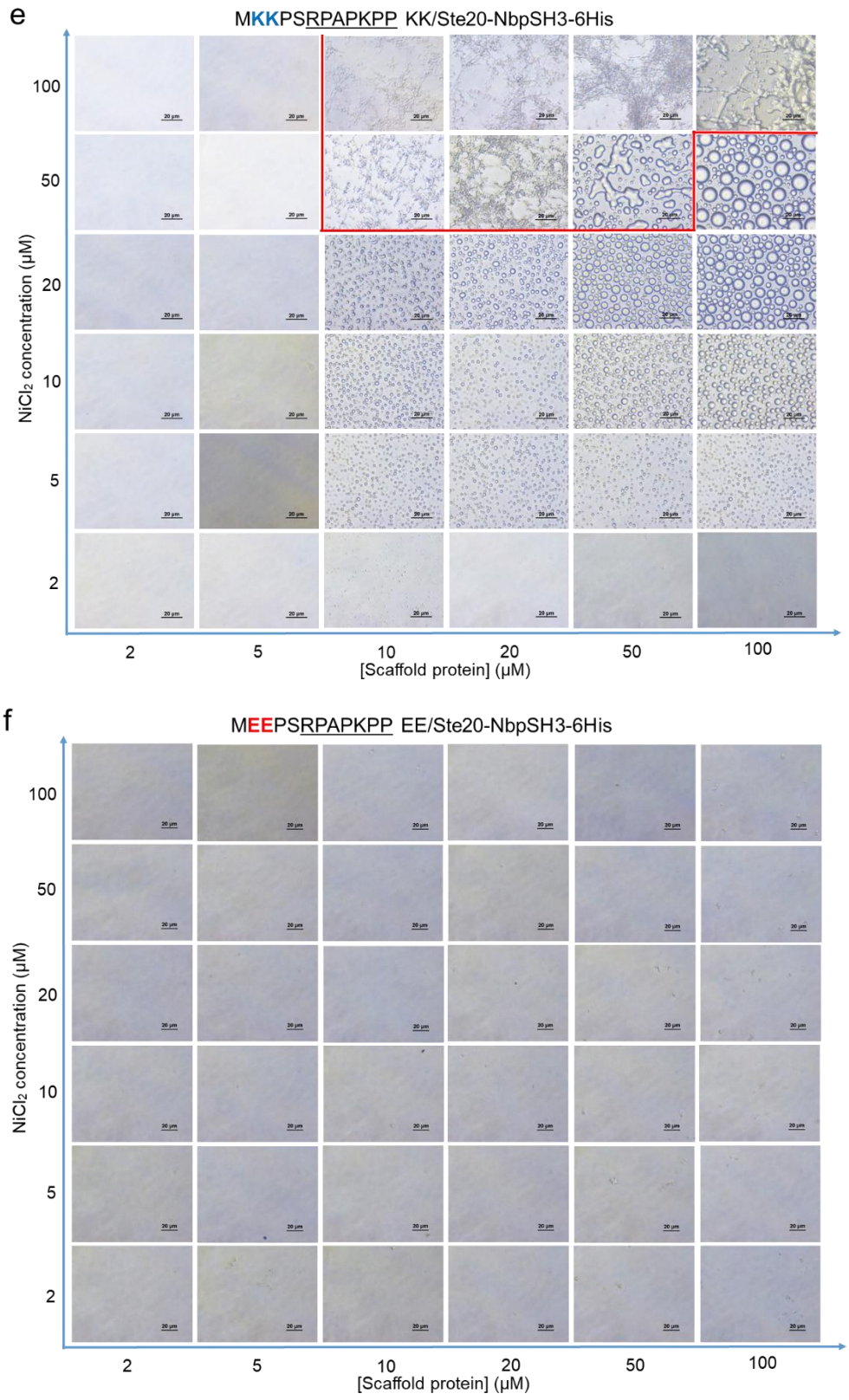

Supplementary Figure 16 Optical images of phase separation diagrams of ligand mutated scaffold proteins. Mutated ligand sequences are shown above images. Phase diagram images of Fig. 4. Scale bars: 10 μm. Images were taken after 24 h upon Ni^{2+} addition.

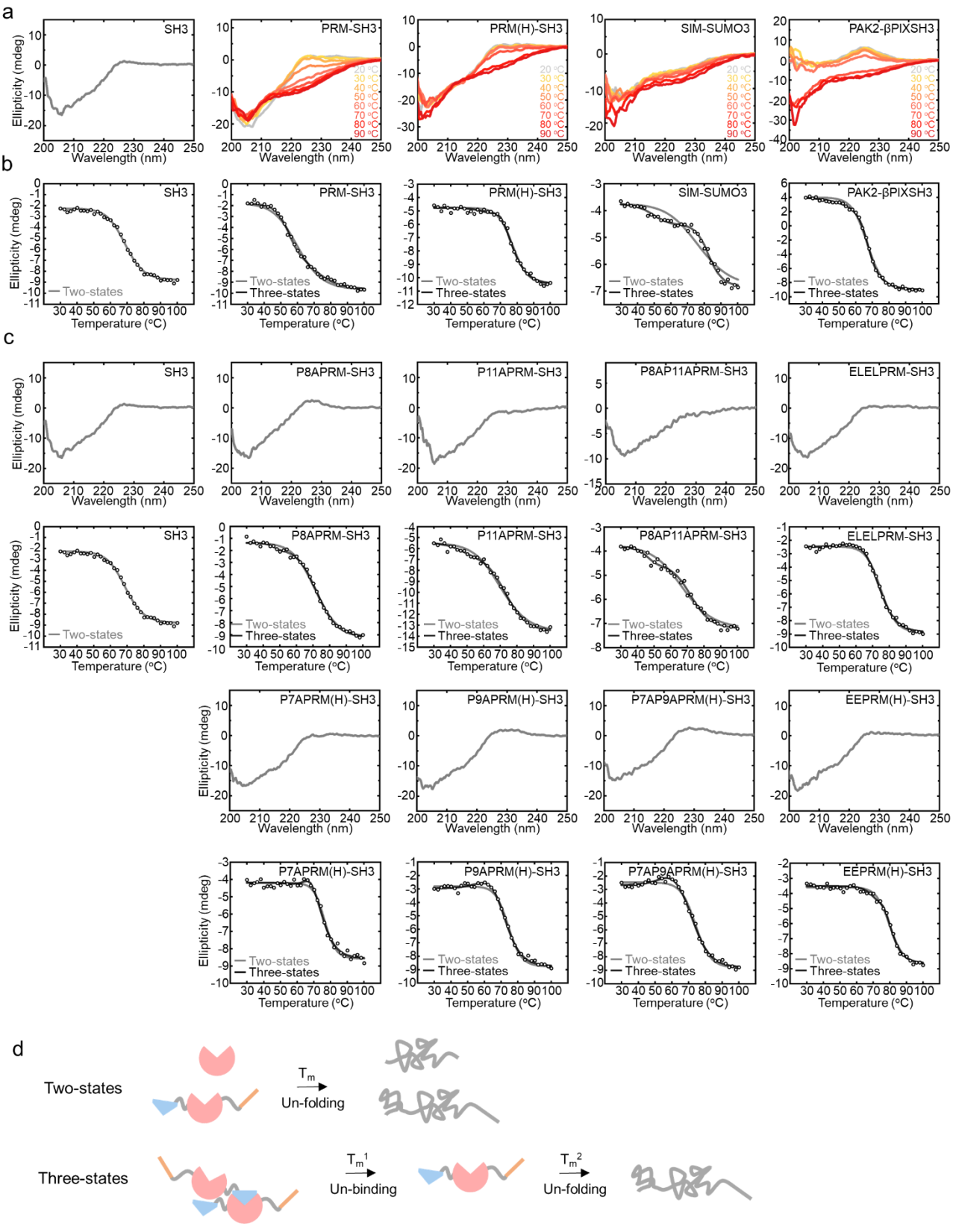

Supplementary Figure 17 Temperature-variable circular dichroism (CD) analysis of various scaffold proteins. (continue)

	Two-states	Three-states	
Protein	T_m (°C)	T_m^1 (°C)	T_m^2 (°C)
SH3	68.83 ± 1.74		
PRM-SH3	60.09 ± 1.73	53.84 ± 0.57	66.68 ± 3.51
P8APRM-SH3	71.32 ± 1.51	45.73 ± 3.18	72.76 ± 0.74
P11APRM-SH3	70.65 ± 0.83	48.64 ± 3.22	73.55 ± 1.92
P8AP11APRM-SH3	68.43 ± 0.34	46.89 ± 5.16	72.67 ± 1.68
ELELPRM-SH3	74.96 ± 0.55	62.94 ± 3.41	71.16 ± 0.67
PRM(H)-SH3	77.51 ± 1.11	66.54 ± 0.71	73.47 ± 0.78
P7APRM(H)-SH3	76.55 ± 0.44	64.46 ± 1.09	73.68 ± 1.40
P9APRM(H)-SH3	74.36 ± 1.06	59.84 ± 0.34	71.50 ± 0.99
P7AP9APRM(H)-SH3	74.59 ± 0.97	59.11 ± 1.20	72.47 ± 0.67
EEPRM(H)-SH3	79.96 ± 0.70	73.81 ± 1.59	77.47 ± 0.62
SIM-SUMO3	75.43 ± 1.69	48.63 ± 5.28	82.89 ± 1.86
PAK2-βPIXSH3	67.03 ± 0.88	65.89 ± 0.34	67.50 ± 1.16

Supplementary Figure 17 Temperature-variable circular dichroism (CD) analysis of various scaffold proteins. (a) Ellipticity profiles (from 200 nm to 250 nm) and (b) ellipticity changes at 222 nm as a function of temperature of LLPS scaffold proteins and free SH3. (c) Ellipticity profiles and changes at 222 nm for Pro-to-Ala and acidic mutation scaffolds. Two-fitting lines (two-state in gray and three-state in black) are indicated. (d) Schematic diagram of two-state and three-state transition models. Calculated unfolding T_m in a two-state transition (folding/unfolding) model and scaffold unbinding T_m^1 and unfolding T_m^2 in a three-state transition (protein unbinding and unfolding) model are given in the below table. All proteins were analyzed at 20 μM concentration in 50 mM sodium phosphate pH 7.4. S.D. n = 3.

Note: Ellipticity profiles were mostly unchanged by tested mutations, indicating structural stability of various binding peptide mutants. Mutations to the binding peptides (PRM and PRM(H)) rather than folded globular domain (SH3) might have only a minimal effects on protein folding/stability. On the other hand, T_m (particularly T_m^1) values were widely varied by mutations. For example, T_m^1 values clearly decreased by (binding weakening) P-to-A mutations, while increased by (binding strengthening) K-to-E mutations (Supplementary Figs. 14 and 17). Raw data and thermodynamic parameters are given in Source Data.

Data analysis: The data fitting was conducted by following the procedures from a previous report[1] with slight modification for a three-state model. The midpoint transition temperature (T_m) of un-

folding was calculated by fitting measured ellipticities at 222 nm at a given temperature to the calculated ellipticity. A two-state transition model was used for a single T_m calculation.

$$\mathrm{F} \overset{K}{\leftrightarrow} \mathrm{U},\ K = [U]/[F] = e^{-\Delta G/RT}, \tag{1}$$

where [F] and [U] are the concentrations of folded and unfolded proteins, respectively.

$$\alpha = [F]/([F] + [U]) = \ 1/(1 + K) = (\theta_t - \theta_U)/(\theta_F - \theta_U), \tag{2}$$

where α is the fraction of folded proteins, θ_t is a measured ellipticity at any temperature, θ_F is the ellipticity where 100 % of proteins exist in a folded form, and θ_U is the ellipticity where 100 % of proteins exist in an unfolded form.

Since ΔC_p is difficult to estimate from CD measurements, we set ΔC_p = 0 in this analysis.

$$\Delta \mathrm{G} = \ \Delta \mathrm{H}(1 - T/T_m) - \Delta C_p((T_m - T) + Tln(T/T_m)) \ \approx \ \Delta \mathrm{H}(1 - T/T_m), \tag{3}$$

where the midpoint transition temperature of unfolding T_m is the temperature at K = 1.

A three-state transition model was used to consider both un-binding T_m^1 (e.g. interactions between PRM and SH3) and un-folding T_m^2 (e.g. SH3) processes (Supplementary Fig 17d).

$\mathrm{D} \overset{K_1}{\leftrightarrow} 2\mathrm{M} \overset{K_2}{\leftrightarrow} 2\mathrm{U}$ (D: dimer, M: monomer, U: un-folded monomer); Three-state equilibrium was simplified with two independent equilibrium states in our model.

$$\mathrm{D} \overset{K_1}{\leftrightarrow} 2\mathrm{M},\ \text{and}\ \ \mathrm{M} \overset{K_2}{\leftrightarrow} \mathrm{U}$$

For the simple modeling, we assumed that two equilibriums are independently governed by given equilibrium constants, and each equilibrium shift also contributes to the change of ellipticity with fraction γ_1 and γ_2 $(\gamma_1 + \gamma_2 = 1)$.

$$K_1 = [M]^2/[D] = [M]([M]/[D]) = [M]\left(e^{-\Delta G_1/RT}\right), \text{and}\ \ K_2 = [U]/[M] = e^{-\Delta G_2/RT} \tag{4}$$

where [M], [D], and [U] are the concentrations of monomer, dimer, and un-folded monomer proteins (when fitting K_1, we set [M] $\approx$ the initial total protein concentration 20 μM as a constraint for ease of fitting).

$$\alpha_1 = 2\,[D]/(2[D] + [M])\ \text{ and }\ \alpha_2 = [M]/([M] + [U])$$

$$(\alpha_1\gamma_1 + \alpha_2\gamma_2) = \ (\theta_t - \theta_U)/(\theta_D - \theta_U), \tag{5}$$

where α_1 is the fraction of monomeric proteins (or domains) which exists in dimeric forms in the $\mathrm{D} \overset{K_1}{\leftrightarrow} 2\mathrm{M}$ two-state system, α_2 is the fraction of folded monomeric proteins in the $\mathrm{M} \overset{K_2}{\leftrightarrow} \mathrm{U}$ two-state system, θ_t is a measured ellipticity at any temperature, θ_D is the ellipticity where 100 % of proteins exist in a dimeric form, and θ_U is the ellipticity where 100 % of proteins exist in monomeric and unfolded forms.

Again, we set all ΔC_p = 0 in this analysis.

$$\Delta G_1 = \Delta H_1(1 - T/T_{m^1}) - \Delta C_{p^1}((T_{m^1} - T) + Tln(T/T_{m^1})) \approx \Delta H_1(1 - T/T_{m^1}), \quad (6)$$

$$\Delta G_2 = \Delta H_2(1 - T/T_{m^2}) - \Delta C_{p^2}((T_{m^2} - T) + Tln(T/T_{m^2})) \approx \Delta H_2(1 - T/T_{m^2}), \quad (7)$$

where the midpoint transition temperature of un-binding (dissociation) T_{m^1} is the temperature at K_1 = 1, and the midpoint transition temperature of monomer un-folding T_{m^2} is the temperature at K_2 = 1. Estimated ellipticity calculations and curve fittings were carried out by using a Excel® (Microsoft) nonlinear least squares analysis tool with given initial parameters (ΔH, θ_F, θ_D and θ_U) based on CD and ITC experiment results.

The Fitting data are provided in Source Data.

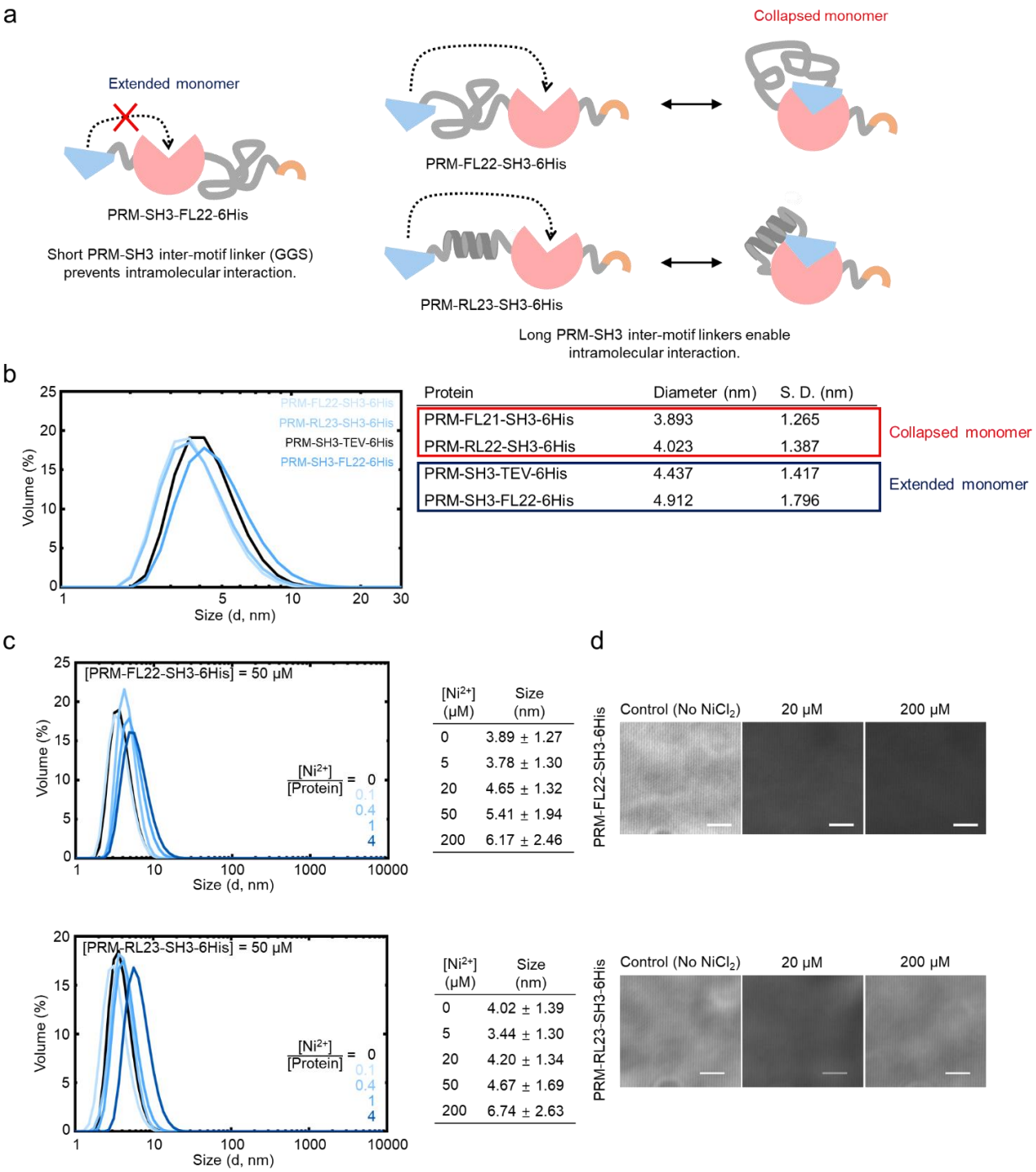

Supplementary Figure 18 Inter-motif linkers between PRM and SH3 (a) Schematic representations of PRM-SH3-Linker-6His with an extended monomer structure (left) and PRM-Linker-SH3-6His with a collapsed monomer structure. (b) DLS size distribution profiles of PRM-SH3 linker variants. Average sizes of are indicated in the right table. s.d. from n = 3. (c) DLS size distribution profiles of PRM-FL22-SH3 and PRM-RL23-SH3 with varying ratios of Ni^{2+}. (d) Optical microscopy images of 50 μM PRM-FL22-SH3 (upper) and PRM-RL23-SH3 (lower) with 20 μM or 200 μM $NiCl_2$. Images were taken after 12 h incubation at 25 ºC upon LLPS. Scale bars: 10 μm.

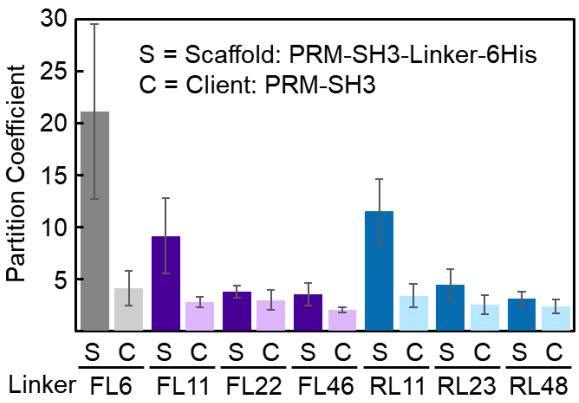

Supplementary Figure 19 Scaffold and client PC values for various linker added scaffold proteins. 100 μM of scaffold proteins were mixed with 50 μM $NiCl_2$, and condensates were imaged after 30 min upon $NiCl_2$ addition. Error bars: 1 s.d. from triplicate experiments with at least 195 condensates.

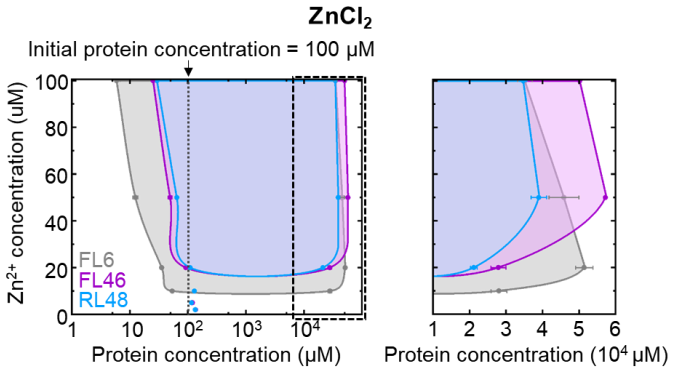

[Zn^{2+}] (μM)	PRM-SH3-FL6		PRM-SH3-FL46		PRM-SH3-RL48	
	[Dilute] (μM)	[Dense] (μM)	[Dilute] (μM)	[Dense] (μM)	[Dilute] (μM)	[Dense] (μM)
2	-	-	-	-	-	-
5	-	-	-	-	-	-
10	53.6 ± 2.07	28000 ± 2160	-	-	-	-
20	35.3 ± 1.30	51400 ± 2360	91.8 ± 4.72	27900 ± 2170	109 ± 1.81	21200 ± 932
50	12.4 ± 1.24	45900 ± 4090	49.3 ± 3.73	57200 ± 207	64.4 ± 1.17	39000 ± 2120
100	5.88 ± 0.860	35100 ± 2000	25.1 ± 1.29	50200 ± 318	29.3 ± 0.0978	34700 ± 939

Supplementary Figure 20 The phase diagrams of PRM-SH3-Linker-6His with dense and dilute phase protein concentrations as a function of Zn^{2+}. Left arms exhibit dilute phase concentrations and right arms for dense phase concentrations of the scaffold (PRM-SH3-6His) protein. The magnified version of the right arms (dash box in the left diagram) is drawn (right diagram). Concentrations are summarized in the below table. S.D. from at least 2 independent experiments. The FL6 data are same as Supplementary Fig. 10, but included for better comparison with the FL46 and RL48 data.

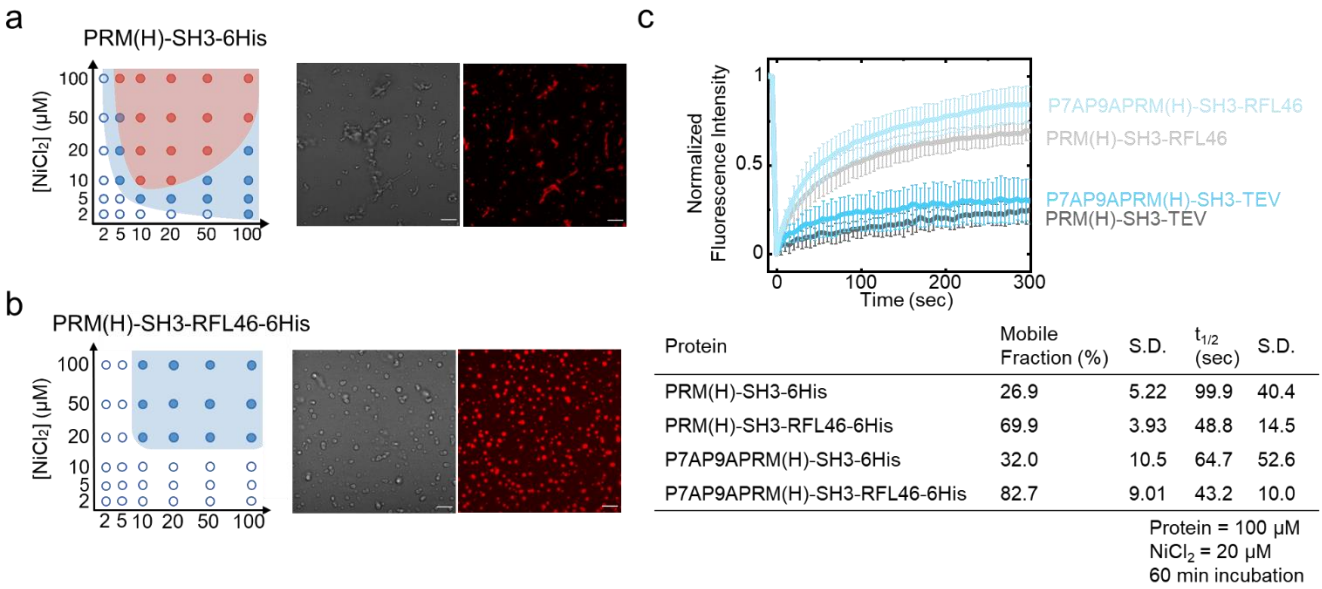

Protein	Mobile Fraction (%)	S.D.	$t_{1/2}$ (sec)	S.D.
PRM(H)-SH3-6His	26.9	5.22	99.9	40.4
PRM(H)-SH3-RFL46-6His	69.9	3.93	48.8	14.5
P7AP9APRM(H)-SH3-6His	32.0	10.5	64.7	52.6
P7AP9APRM(H)-SH3-RFL46-6His	82.7	9.01	43.2	10.0

Protein = 100 μM
$NiCl_2$ = 20 μM
60 min incubation

Supplementary Figure 21 Condensate morphology shift by scaffold linker addition. (a) A phase diagram and optical images of PRM(H)-SH3-6His condensates (protein 100 μM and Ni^{2+} 20 μM). DIC and optical images were taken after 24 h upon condensate formation. (b) A phase diagram and optical images of PRM(H)-SH3-RFL46-6His condensates (protein 100 μM and Ni^{2+} 20 μM). Scale bars: 10 μm. (c) FRAP recovery profiles of PRM(H)-SH3-6His linker and Pro-to-Ala scaffold variants. S.D. from triplicate experiments with at least 10 condensates.

Note: Pro-to-Ala mutated P7AP9APRM(H)-SH3-6His (Fig. 4b) condensates also showed increased diffusivity by inserting the long RFL46 peptide linker.

RFL linker: GSKESGSVSSEQLAQFRSLDEFEGKSSGSGSESKSTETSGGSGSLE

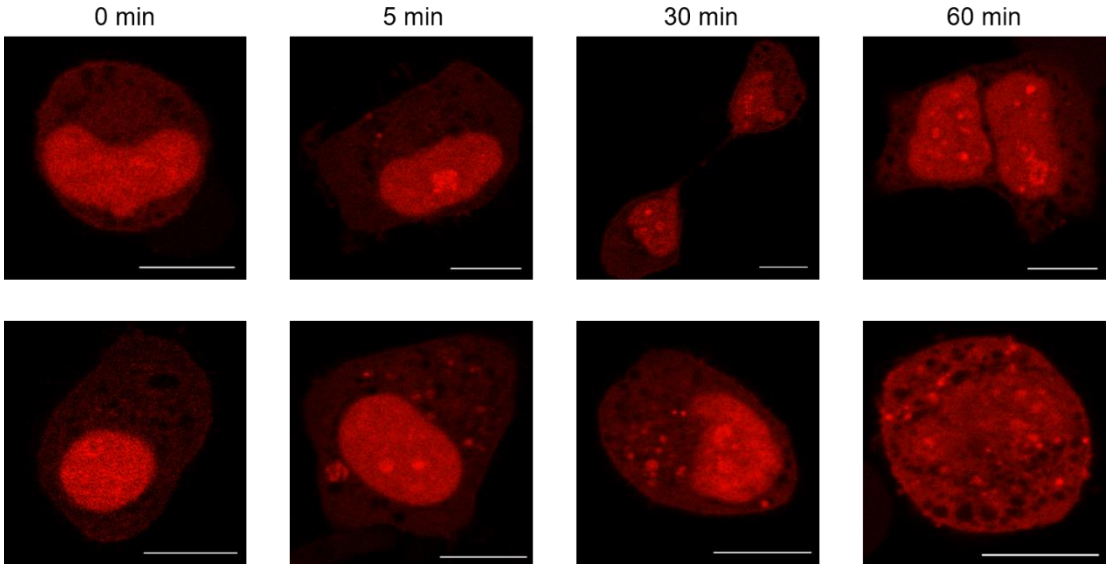

Supplementary Figure 22 Time-dependent increase of the Zn^{2+}-mediated formation of mCh-PRM-SH3-6His condensates in HeLa cells. Scale bars: 10 μm.

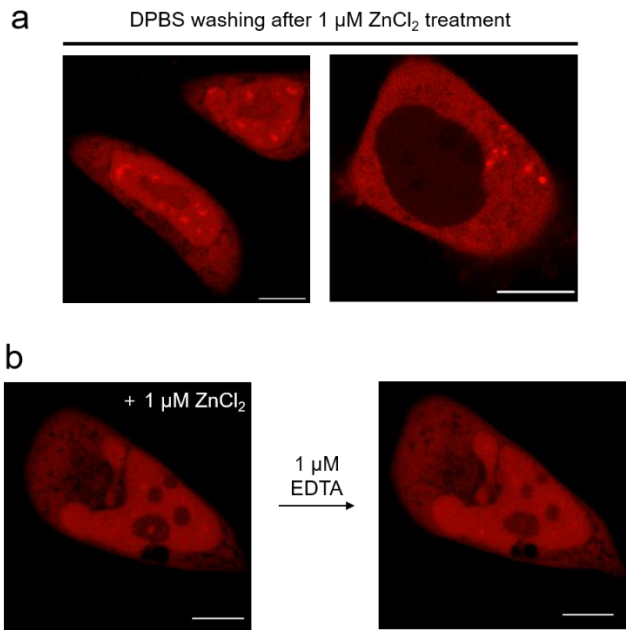

Supplementary Figure 23 Irreversible formation of Zn^{2+}-mediated mCh-PRM-SH3-6His puncta. (a) Fluorescence images of mCh-PRM-SH3-6His condensates in HeLa cells with DPBS washing after 1 μM of $ZnCl_2$ treatment. (b) Fluorescence images of mCh-PRM-SH3-6His condensates in HeLa cells with EDTA treatment after 1 μM of $ZnCl_2$ treatment. Scale bars: 10 μm.

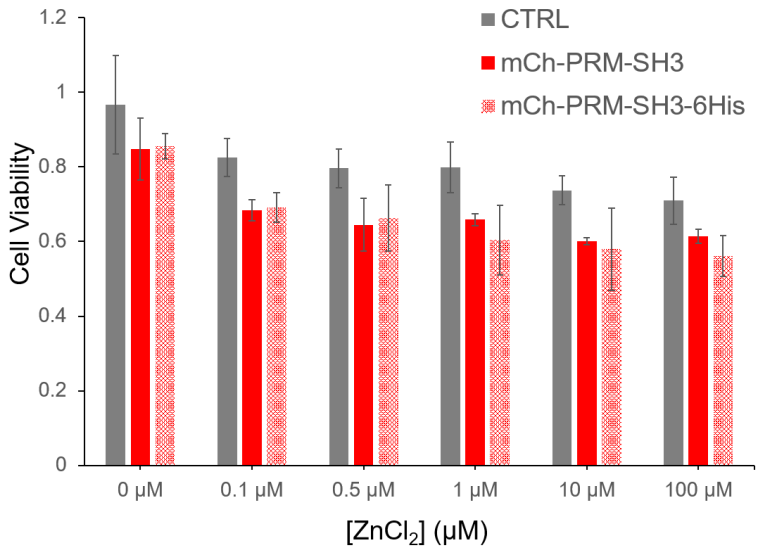

Supplementary Figure 24 Effects of mCherry-PRM-SH3 protein and puncta formation in HeLa cells as a function of $ZnCl_2$ concentration measured by MTT assay. S. D. n = 3

Supplementary Tables

Supplementary Table 1 Partition coefficients of four scaffold proteins. (Data for Fig. 1f)

Client	P.C.	S.D.
PRM-SH3	12.1	2.31
PRM(H)-SH3-TEV	31.8	13.1
SIM-SUMO3	4.19	0.46
PAK2-βPIXSH3	12.8	3.46

[Protein] = 100 μM, [Ni^{2+}] = 20 μM (50 μM for SIM-SUMO3), 60 min incubation
Standard deviation (S.D.) from three independent experiments.

Supplementary Table 2 Mobile fraction and $t_{1/2}$ values of FRAP analysis for four scaffold proteins (Data for Fig. 1g)

Protein	Mobile Fraction (%)	S.D.	$t_{1/2}$ (sec)	S.D.
PRM-SH3	63.7	7.66	78.3	18.5
PRM(H)-SH3-TEV	26.9	5.22	99.9	40.4
SIM-SUMO3	35.4	7.25	77.9	22.4
PAK2-βPIXSH3	7.74	3.02	58.3	53.2

[Protein] = 100 μM, [Ni^{2+}] = 20 μM (50 μM for SIM-SUMO3), 60 min incubation
S.D. from three independent experiments.

Supplementary Table 3 Mobile fraction and $t_{1/2}$ values of FRAP analysis for four metal ions (Data for Fig. 2b)

Metal ion	Mobile Fraction (%)	S.D	$t_{1/2}$ (sec)	S.D.
Ni^{2+}	36.7	21.9	193	119
Zn^{2+}	75.8	8.93	96.4	66.7
Co^{2+}	68.6	10.0	137	48.3
Cu^{2+}	85.8	6.08	45.9	14.5

[Protein] = 100 μM, [Metal ion] = 100 μM, 60 min incubation
S.D. from three independent experiments.

Supplementary Table 4 Mobile fraction and $t_{1/2}$ values of FRAP analysis for linker added PRM-SH3-Linker-6His scaffold proteins (Data for Fig. 5c)

Inter-motif linker	Mobile Fraction (%)	S.D	$t_{1/2}$ (sec)	S.D.
FL6	26.9	6.56	115	61.3
FL11	50.8	7.00	109	23.0
FL22	70.8	4.33	37.7	6.72
FL46	81.3	8.93	34.8	4.04
RL11	47.6	5.88	91.7	19.5
RL23	86.0	3.44	29.4	6.27
RL48	73.4	5.73	28.9	5.85

[Protein] = 100 μM, [Ni^{2+}] = 50 μM, 30 min incubation
S.D. from three independent experiments.

Supplementary Table 5 Mobile fraction and $t_{1/2}$ values of FRAP analysis for the PRM-SH3 client inside linker added PRM-SH3-Linker-6His condensates (Data for Fig. 5c)

Inter-motif linker	Mobile Fraction (%)	S.D	$t_{1/2}$ (sec)	S.D.
FL6	61.7	6.08	63.8	11.8
FL11	74.6	5.68	28.3	3.57
FL22	85.7	4.35	22.1	4.75
FL46	82.1	3.64	11.2	2.71
RL11	74.8	8.17	26.1	3.41
RL23	86.9	6.05	12.7	5.00
RL48	85.2	5.25	10.8	3.43

[Protein] = 100 μM, [Ni^{2+}] = 50 μM, 30 min incubation
S.D. from three independent experiments.

Supplementary Table 6 Mobile fraction and $t_{1/2}$ values of FRAP analysis for cellular condensates (Data for Fig. 6)

Protein	Mobile Fraction (%)	S.D.	$t_{1/2}$ (sec)	S.D.
mCh-PRM-SH3-6His	92.8	21.1	53.8	32.6
mCh-PRM(H)-SH3-6His	41.5	21.9	31.9	25.4

[Zn^{2+}] = 10 μM, 60 min incubation
S.D. from 6 – 8 cellular droplets.

Protein Sequences

Blue: peptide ligand, Red: receptor, Purple: receptor-6His inter-motif linker (TEV protease site underlined), Green: additional motifs or proteins

Protein/Ligand	Amino acid sequence	Note
(PRM variant)-SH3-6His	(PRMvariant)GGSDLNMPAYVKFNYMAEREDELSLIKGTKVIVMEKSSDGWWRGSYNGQVGWFPSNYVTEEGDSPLGSENLYFQGLEHHHHHH	PRM: Human Abl1 residues 606-618 SH3: Human Nck1 second SH3 domain residues 106-168, C169S mutation to prevent disulfide bond formation[2]
PRM	MKKKKTAPTPPKRS	PRM (wild-type)
P8APRM	MKKKKTAATPPKRS	PRM variant
P11APRM	MKKKKTAPTPAKRS	PRM variant
P8AP11APRM	MKKKKTAATPAKRS	PRM variant
ELEL/PRM	MELELTAPTPPKRS	PRM variant
FIFI/PRM	MFIFITAPTPPKRS	PRM variant
PRM-(Linker)-SH3-6His	MKKKKTAPTPPKRS(Linker)DLNMPAYVKFNYMAEREDELSLIKGTKVIVMEKSSDGWWRGSYNGQVGWFPSNYVTEEGDSPLLEHHHHHH	
PRM-SH3-(Linker)-6His	MKKKKTAPTPPKRSGGSDLNMPAYVKFNYMAEREDELSLIKGTKVIVMEKSSDGWWRGSYNGQVGWFPSNYVTEEGDSPL(Linker)HHHHHH	
FL6	GSGSLE	Linker variant
FL11	GSGGSGSGSLE	Linker variant
FL21	GSGGSGGSGSGSGGSGGSGSL	Linker variant
FL22	GSGGSGGSGSGSGGSGGSGSLE	Linker variant
FL46	GSGGSGGSGSGSGGSGGSGGSGSGGSGGSGGSGSGSGGSGSLE	Linker variant
RL11	GSEAAAKGSLE	Linker variant
RL22	GSEAAAKEAAAKEAAAKGSGSL	Linker variant
RL23	GSEAAAKEAAAKEAAAKGSGSLE	Linker variant
RL48	GSEAAAKEAAAKEAAAKEAAAKEAAAKEAAAKEAAAKEAAAKGSGSLE	Linker variant
RFL45	GSKESGSVSSEQLAQFRSLDEFEGKSSGSGSESKSTETSGGSGSL	Linker variant
RFL46	GSKESGSVSSEQLAQFRSLDEFEGKSSGSGSESKSTETSGGSGSLE	Linker variant
(PRM(H) variant)-SH3-6His	(PRM(H)variant)GGSDLNMPAYVKFNYMAEREDELSLIKGTKVIVMEKSSDGWWRGSYNGQVGWFPSNYVTEEGDSPLGSENLYFQGLEHHHHHH	PRM(H): Human Disks large-associated protein 2 residues 610-623[2]
PRM(H)	MKKTPPPVPPRTTSK	PRM(H) (wild-type)
P7APRM(H)	MKKTPPAVPPRTTSK	PRM(H) variant
P9APRM(H)	MKKTPPPVAPRTTSK	PRM(H) variant
P7AP9APRM(H)	MKKTPPAVAPRTTSK	PRM(H) variant
EE/PRM(H)	MEETPPPVPPRTTSK	PRM(H) variant
FI/PRM(H)	MFITPPPVPPRTTSK	PRM(H) variant

(PRM(H) variant)-SH3-RFL46-6His	(PRM(H)variant)GGSDLNMPAYVKFNYMAEREDELSLIKGTKVIVMEKSSDGWWRGSYNGQVGWFPSNYVTEEGDSPLGSKESGSVSSEQLAQFRSLDEFEGKSSGSGSESKSTETSGGSGSLEHHHHHH	For Supplementary Fig. 14
SIM-SUMO-6His	MKVDVIDLTIESSSDEEEDPPAKRGSMSEEKPKEGVKTENDHINLKVAGQDGSVVQFKIKRHTPLSKLMKAYCERQGLSMRQIRFRFDGQPINETDTPAQLEMEDEDTIDVFQQQTVVGSENLYFQGLEHHHHHH	SIM: Human E3 SUMO-protein ligase PIAS2 residues 466-488 SUMO: Human Small ubiquitin-related modifier 3 residues 1-92, G91V and G92V mutations to prevent processing by proteases[3]
PAK2-βPIXSH3-6His	MEETAPPVIAPRPDHTKSIYTRSVIGGSGPLGSVVRAKFNFQQTNEDELSFSKGDVIHVTRVEEGGWWEGTHNGRTGWFPSNYVREIGSENLYFQGLEHHHHHH	PAK2: Human Serine/threonine-protein kinase PAK 2 residues 176-199 βPIXSH3: Rat Rho guanine nucleotide exchange factor 7 residues 10-63[4]
(Ste20 variant)-NbpSH3-6His	(Ste20variant)GGSIVNQRAVALYDFEPENDNELRLAEGDIVFISYKHGQGWLVAENESGSKTGLVPEEFVSYIQPEGSENLYFQGLEHHHHHH	Ste20: Yeast Serine/threonine-protein kinase STE20 residues 470~480 NbpSH3: Yeast NAP1-binding protein residues 110-172[5]
Ste20	MFIPSRPAPKPP	Ste20 (wild-type)
KK/Ste20	MKKPSRPAPKPP	Ste20 variant
EE/Ste20	MEEPSRPAPKPP	Ste20 variant
D7NSpyTag-PRM-SH3-6His	MAHIVMVNAYKPTKGGSKKKKTAPTPPKRSGGSDLNMPAYVKFNYMAEREDELSLIKGTKVIVMEKSSDGWWRGSYNGQVGWFPSNYVTEEGDSPLGSENLYFQGLEHHHHHH	SpyTag D7N mutant
GFP-6His	MKGEELFTGVVPILVELDGDVNGHEFSVRGEGEGDATIGKLTLKFICTTGKLPVPWPTLVTTLTYGVQCFSRYPDHMKRHDFFKSAMPEGYVQERTISFKDDGKYKTRAVVKFEGDTLVNRIELKGTDFKEDGNILGHKLEYNFNSHDVYITADKQENGIKAEFTVRHNVEDGSVQLADHYQQNTPIGDGPVLLPDNHYLSTQTVLSKDPNEKRDHMVLHEYVNAAGITGSENLYFQGLEHHHHHH	GFP: The (-9) charge variant of superfolder GFP[6]
GFP-PRM-6His	MKKKKTAPTPPKRSGGSKGEELFTGVVPILVELDGDVNGHEFSVRGEGEGDATIGKLTLKFICTTGKLPVPWPTLVTTLTYGVQCFSRYPDHMKRHDFFKSAMPEGYVQERTISFKDDGKYKTRAVVKFEGDTLVNRIELKGTDFKEDGNILGHKLEYNFNSHDVYITADKQENGIKAEFTVRHNVEDGSVQLADHYQQNTPIGDGPVLLPDNHYLSTQTVLSKDPNEKRDHMVLHEYVNAAGITGSENLYFQGLEHHHHHH	

GFP-PRM-SH3-6His	MKGEELFTGVVPILVELDGDVNGHEFS VRGEGEGDATIGKLTLKFICTTGKLPVP WPTLVTTLTYGVQCFSRYPDHMKRHDF FKSAMPEGYVQERTISFKDDGKYKTRA VVKFEGDTLVNRIELKGTDFKEDGNILG HKLEYNFNSHDVYITADKQENGIKAEFT VRHNVEDGSVQLADHYQQNTPIGDGPV LLPDNHYLSTQTVLSKDPNEKRDHMVL HEYVNAAGITGSKKKKTAPTPPKRSGGS DLNMPAYVKFNYMAEREDELSLIKGTK VIVMEKSSDGWWRGSYNGQVGWFPSN YVTEEGDSPLGSENLYFQGLEHHHHHH	
GFP-SpyCatcher-6His	MKGEELFTGVVPILVELDGDVNGHEFS VRGEGEGDATIGKLTLKFICTTGKLPVP WPTLVTTLTYGVQCFSRYPDHMKRHDF FKSAMPEGYVQERTISFKDDGKYKTRA VVKFEGDTLVNRIELKGTDFKEDGNILG HKLEYNFNSHDVYITADKQENGIKAEFT VRHNVEDGSVQLADHYQQNTPIGDGPV LLPDNHYLSTQTVLSKDPNEKRDHMVL HEYVNAAGITGSGAMVDTLSGLSSEQG QSGDMTIEEDSATHIKFSKRDEDGKELA GATMELRDSSGKTISTWISDGQVKDFYL YPGKYTFVETAAPDGYEVATAITFTVNE QGQVTVNGKATKGDAHIENLYFQGLEH HHHHH	SpyCatcher: Streptococcus pyogenes fibronectin binding protein Fbab-B (PDB:2x5p) residues -2-113[7]
mCherry-PRM-SH3-6His	MVSKGEEDNMAIIKEFMRFKVHMEGSV NGHEFEIEGEGEGRPYEGTQTAKLKVTK GGPLPFAWDILSPQFMYGSKAYVKHPAD IPDYLKLSFPEGFKWERVMNFEDGGVV TVTQDSSLQDGEFIYKVKLRGTNFPSDG PVMQKKTMGWEASSERMYPEDGALKG EIKQRLKLKDGGHYDAEVKTTYKAKKP VQLPGAYNVNIKLDITSHNEDYTIVEQY ERAEGRHSTGGMDELYKGGSKKKTAP TPPKRSGGSDLNMPAYVKFNYMAERED ELSLIKGTKVIVMEKSSDGWWRGSYNG QVGWFPSNYVTEEGDSPLLEHHHHHH	For cell experiments
mCherry-PRM(H)-SH3-6His	MVSKGEEDNMAIIKEFMRFKVHMEGSV NGHEFEIEGEGEGRPYEGTQTAKLKVTK GGPLPFAWDILSPQFMYGSKAYVKHPAD IPDYLKLSFPEGFKWERVMNFEDGGVV TVTQDSSLQDGEFIYKVKLRGTNFPSDG PVMQKKTMGWEASSERMYPEDGALKG EIKQRLKLKDGGHYDAEVKTTYKAKKP VQLPGAYNVNIKLDITSHNEDYTIVEQY ERAEGRHSTGGMDELYKGGSKKTPPPV PPRTTSKGGSDLNMPAYVKFNYMAERE DELSLIKGTKVIVMEKSSDGWWRGSYN GQVGWFPSNYVTEEGDSPLLEHHHHHH	For cell experiments

References

1. Greenfield, N.J. Using circular dichroism collected as a function of temperature to determine the thermodynamics of protein unfolding and binding interactions. *Nat. Protoc.* **1**, 2527–2535 (2006).
2. Li, P. et al. Phase transitions in the assembly of multivalent signalling proteins. *Nature* **483**, 336-340 (2012).
3. Banani, S.F. et al. Compositional Control of Phase-Separated Cellular Bodies. *Cell* **166**, 651-663 (2016).
4. Hoelz, A. et al. Crystal structure of the SH3 domain of betaPIX in complex with a high affinity peptide from PAK2. *J. Mol. Biol.* **358**, 509-522 (2006).
5. Gorelik, M. & Davidson, A.R. Distinct peptide binding specificities of Src homology 3 (SH3) protein domains can be determined by modulation of local energetics across the binding interface. *J. Biol. Chem.* **287**, 9168-9177 (2012).
6. Kim, Y.E., Kim, Y.N., Kim, J.A., Kim, H.M. & Jung, Y. Green fluorescent protein nanopolygons as monodisperse supramolecular assemblies of functional proteins with defined valency. *Nat. Commun.* **6**, 7134 (2015).
7. Zakeri, B. et al. Peptide tag forming a rapid covalent bond to a protein, through engineering a bacterial adhesin. *Proc. Natl. Acad. Sci. USA* **109**, E690-E697 (2012).